Journal of Zhejiang University SCIENCE A
ISSN 1673-565X (Print); ISSN 1862-1775 (Online)
www.zju.edu.cn/jzus; www.springerlink.com
E-mail: jzus@zju.edu.cn

A novel three-component hybrid-integrated optical accelerometer based on a Mach-Zehnder interferometer with a $LiNbO_3$ photoelastic waveguide*

Dong-lin TANG†1, Xiao-dong ZHANG[1], Guang-hui ZHAO[1], Zhi-yong DAI[2], Xin LAI[1], Feng GUO[1]

([1]*MOE Key Laboratory for Petroleum-Gas Equipment, Southwest Petroleum University, Chengdu 610500, China*)

([2] *School of Optoelectronic Information, University of Electronic Science and Technology, Chengdu 610054, China*)

†E-mail: xnsytdl@yahoo.com.cn

Received June 5, 2008; Revision accepted Oct. 16, 2008; Crosschecked Feb. 25, 2009

Abstract: An investigation of the properties of a $LiNbO_3$ photoelastic waveguide via the acceleration-induced effect is presented. A novel three-component hybrid-integrated optical accelerometer based on a Mach-Zehnder interferometer with a $LiNbO_3$ photoelastic waveguide has been designed, which is capable of detecting seismic acceleration in high-accuracy seismic exploration. The Mach-Zehnder interferometer was successfully fabricated and a lighting test used to check its quality. The frequency response characteristic of the accelerometer was measured. The accelerometer with a resonant frequency of 3549 Hz was demonstrated to show good linear frequency responding characteristics in the range of 100~3000 Hz. The accelerometer also shows good stability and consistency. Experimental results indicate that the outputs of the on- and cross-axis are 147 and 21.3 mV, respectively.

Key words: Integrated optics, Accelerometer, Photoelastic waveguide, Mach-Zehnder interferometer (MZI)
doi:10.1631/jzus.A0820420 **Document code:** A **CLC number:** TP212

INTRODUCTION

A variety of uniaxial crystals, including $LiNbO_3$, have been found in which the induced photoelastic effect varies linearly with the applied stress field. This phenomenon forms the basis for the science of photoelasticity. Because of its high resolution and low measuring time, some recent work has shown the possibility of using photoelastic effect with photoelastic materials for sensor applications, such as high-strain sensors (Kiesel *et al*., 2006), dynamic tactile sensors (Dubey and Crowder, 2006), and pressure sensors (Guo *et al*., 2004).

There have been several proposals for optical accelerometers based on photoelastic effects using fiber optics (Su *et al*., 1997; Tang *et al*., 2005), but the most common light guiding structures used on optical accelerometers have a high refractive index etched layer (frequently silicon nitride) in a cantilever configuration (Burcham *et al*., 1992). Pavelescu (2001) indicated that the anti-resonant reflecting optical waveguides (ARROW) could be suitable for pressure sensors on the basis of a photoelastic effect. Although accelerometers based on ARROW have been designed (Llobera *et al*., 2004), the devices were extremely fragile and cracked easily because of the complex structure of this waveguide. Ma *et al*.(2007) designed a waveguide accelerometer based on the photoelastic effect of a suspended waveguide, but it was difficult to fabricate the sensor.

In this study, based on the $LiNbO_3$ waveguide photoelastic effect, we propose a novel three-component accelerometer. Three polarizers and two phase modulators are integrated with the Mach-Zehnder interferometer (MZI) fabricated by integrated optics technology on the same $LiNbO_3$ substrate. The

* Project supported by the National Natural Science Foundation of China (No. 40774067) and the Applied Basic Research Program of Sichuan Province, China (No. 07JY029-135)

accelerometer with a resonant frequency of 3549 Hz is demonstrated to work well in the range of 100~3000 Hz. So it provides a high-performance, compact, hybrid-integrated fiber-optic sensor with long-term stability and reliability, which is adapted to mass production. It can be employed to monitor or accurately measure vibrations in various applications such as seismic measurement in geophysical surveys. Here, we describe and characterize the accelerometer we have developed.

SENSOR DESIGN AND PRINCIPLE OF OPERATION

Design of hybrid-integrated optical chip

We designed an interferometric integrated optic accelerometer as an interferometric sensor that offers increased sensitivity and resolution. The MZI on the *x*-cut *y*-propagation substrate (the light axis is along *z*) we have designed is shown in Fig.1. The horizontally polarized laser beam from the laser diode (LD) has an output intensity I and wavelength λ, and passes through a horizontal polarizer, polarizer 1, to ensure that the beam is polarized perpendicular to the stress direction caused by acceleration forces on proof mass 6. After passing through polarizer 1, the beam is divided by a symmetric *y*-branch waveguide, resulting in two separate beams traveling in respective waveguides each with a beam intensity of $I/2$. These two beams are further split by symmetric *y*-branch waveguides forming four separate beams traveling in waveguides 2, 3, 4, and 5 each with intensity of $I/4$. When the proof mass 6 attached to waveguides 2 and 5 is accelerated with acceleration forces in the direction of ΔF, it will stress one waveguide in tension and the other in compression. This changes the index of refraction of these photoelastic waveguides. The phase shift following the variation of the index will be adjusted by external acceleration. The light passing through waveguides 3 and 4, which are not stressed, passes through 90° phase bias elements 7 and 8, respectively.

The light modulated by external acceleration and the phase modulator will pass through polarizers 9 and 10 after being coupled by the branch waveguide. The polarizers are employed to realize and maintain the polarization state of the output lightwaves, and also to filter the optical signals out of detection directions. The light signals are converted to electrical signals by photodetectors 11 and 12. Acceleration is achieved by feeding the electrical signal into a signal processor unit 13.

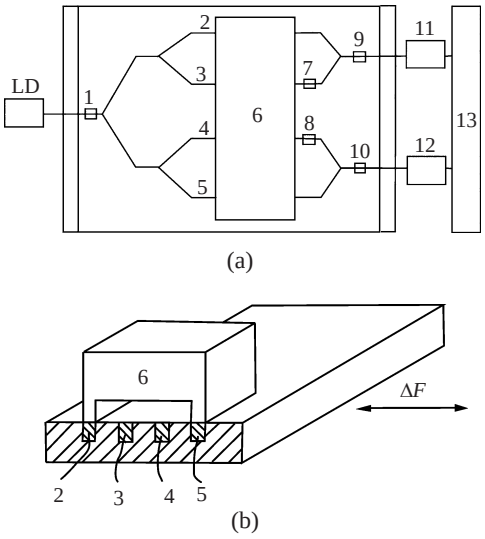

1, 7~10: polarizer; 2~5: waveguide; 6: proof mass;
11, 12: photodetector; 13: signal processor unit

Fig.1 Hybrid-integrated optic chip for acceleration detection. (a) Top view; (b) Side view

Principle of three-component acceleration detection

The acceleration a_k acting on the proof mass can be resolved into a_x, a_y, a_z, and the light travels along the axes as shown in Fig.2. Under the action of the applied acceleration, the small hexahedral element is separated from the sensing material (Fig.3), where σ_y is the normal stress along the *y*-direction, and τ_{yz} and τ_{yx} are shear stresses pointing to the *z*- and *x*-direction, respectively. The normal and shear stresses are expressed as

$$\sigma_y = F_y / (bl) = ma_y / (bl),$$
$$\tau_{yz} = F_z / (bl) = ma_z / (bl),$$
$$\tau_{yx} = F_x / (bl) = ma_x / (bl),$$

where F is the applied force, bl is the contact area of the waveguide, and m is the proof mass. According to Hooke's law, we can obtain the strain of $LiNbO_3$ from the stress as follows:

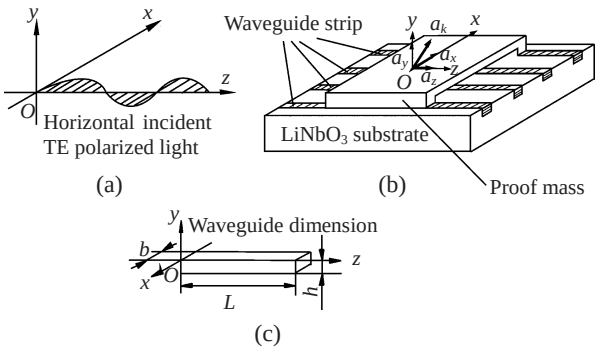

Fig.2 Analysis of the photoelastic effect
(a) TE polarized light; (b) Stress analysis of proof mass waveguide; (c) Waveguide dimension

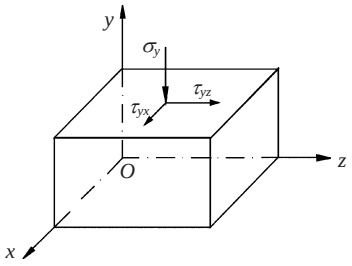

Fig.3 Modeling of the sensing medium

$$\begin{pmatrix}\varepsilon_1\\ \varepsilon_2\\ \varepsilon_3\\ \varepsilon_4\\ \varepsilon_5\\ \varepsilon_6\end{pmatrix}=\begin{pmatrix}s_{11} & s_{12} & s_{13} & s_{14} & 0 & 0\\ 0 & s_{11} & s_{13} & -s_{14} & 0 & 0\\ 0 & 0 & s_{33} & 0 & 0 & 0\\ 0 & 0 & 0 & s_{44} & 0 & 0\\ 0 & 0 & 0 & 0 & s_{44} & 2s_{14}\\ 0 & 0 & 0 & 0 & 0 & 2(s_{11}-s_{12})\end{pmatrix}\begin{pmatrix}0\\ 0\\ \sigma_y\\ \tau_{yz}\\ \tau_{yx}\\ 0\end{pmatrix}. \quad (1)$$

Substituting ε into the photoelastic effect equation of the $LiNbO_3$ waveguide yields

$$\Delta(1/n^2)_i = p_{ik}\varepsilon_j, \quad (2)$$

where $\Delta(1/n^2)_i$ (i=1, 2, …, 6) is the change of the refractive index of the waveguide, ε_j (j=1, 2, …, 6) is a component of the strain, and p_{ik} (i, k=1, 2, …, 6) is the photoelastic tensor.

After obtaining the change of refractive index of the waveguide, we can obtain the phase shift caused by three-dimensional acceleration:

$$\Delta\phi_c = \frac{2\pi}{\lambda}\Delta n_c l, \quad c = x,\ y,\ \text{or } z, \quad (3)$$

where $\Delta\phi_c$ is the phase shift, Δn_c is the change of refractive index. In our design, a typical example may be: light axis ordinary refractive index n_0=2.219, extraordinary refractive index n_e=2.145 when the wavelength of polarized light is 1.3 μm, the waveguide geometry sizes of the sensors are L=10 mm, b=6.5 μm, h=2.5 μm, and the proof mass m=50 g. Substituting these parameters into Eq.(3), we obtain the matrix that shows the relationship between the changes of optical phase of the waveguide and the applied acceleration:

$$\begin{pmatrix}(2.07\times10^{-5}\Delta\phi_x+2.219)^2-0.20\\ (2.07\times10^{-5}\Delta\phi_y+2.219)^2-0.20\\ (2.07\times10^{-5}\Delta\phi_z+2.145)^2-0.22\end{pmatrix}=\begin{pmatrix}-0.057\times10^{-6} & 0.55\times10^{-6} & 0.88\times10^{-3}\\ -0.198\times10^{-6} & -0.24\times10^{-6} & 0.88\times10^{-3}\\ 0.290\times10^{-6} & 0.90\times10^{-6} & -0.03\times10^{-3}\end{pmatrix}\begin{pmatrix}a_x+g\\ a_y\\ a_z\end{pmatrix}.$$

RESULTS FROM THE FABRICATION OF THE MACH-ZEHNDER INTERFEROMETER

Simulation results of optical field

We used the finite difference beam propagation method (FD-BPM) and transparent boundary condition (TBC) method to simulate the lightwave propagation in a y-branching waveguide. The result is shown in Fig.4. The Mach-Zehnder (M-Z) waveguide interferometer we have designed has a good splitting ratio and low loss.

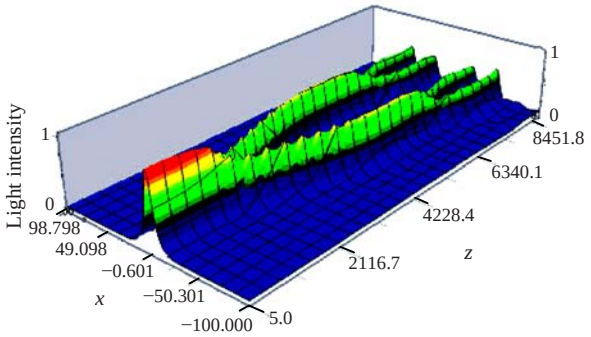

Fig.4 Simulated results of optical field propagation of the Mach-Zehnder interferometer

Ti-sputtered waveguide lineation

The Ti-sputtered waveguide lineation, observed using an OLYMPUS BH-2 microscope (made in Japan) under 20×20 magnification, is shown as Fig.5. The quality of the waveguide lineation is fine and there are no breakpoints.

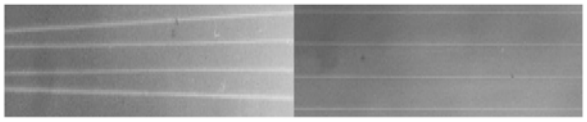

Fig.5 Ti-sputtered waveguide lineation observed using an OLYMPUS BH-2 microscope under 20×20 magnification

Results of lighting test

Light of wavelength 1.3 μm was passed through the waveguides fabricated in the MZI to check the quality of the waveguides. The schematic diagram is shown in Fig.6. Fig.7 gives the diffraction image captured using an infrared video camera (OLYMPUS BH-2, made in Japan). It is obvious that the quality of the waveguides is excellent.

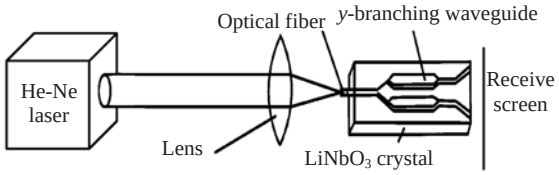

Fig.6 Schematic diagram of the lighting test

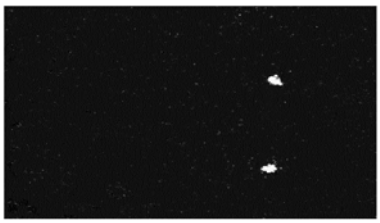

Fig.7 Diffraction image of output light with wavelength 1.3 μm

EXPERIMENTAL RESULTS AND DISCUSSION

Fig.8 shows a schematic drawing of the three-component photoelastic waveguide accelerometer we have designed. The horizontally polarized laser beam from the LD laser is split into three beams to pass through three MZIs, respectively. When arbitrary-direction acceleration forces act on the substrate, the three MZIs can be affected by the accelerations a_x, a_y, a_z along x, y, z directions, respectively. After the variation of acceleration components being converted into the optical phase shift, the light will be transmitted into three PIN photodiodes, which are employed to convert interferometric optical intensity into electric signal. To realize the high-accuracy detection and compensation of the acceleration signal, a digitized alternate current phase tracking (ACPT) homodyne scheme (Cole *et al*., 1982; Dandridge *et al*., 1982) shown in Fig.9, is employed. Firstly, the weak photocurrent is amplified and converted into a voltage signal by a pre-amplifier. Then a bandpass filter is used to remove the direct current signal and increase the signal-to-noise ratio (SNR). Finally, the signal is coupled into a DSP after analog-to-digital (A/D) conversion with an A/D converter. We can obtain the relationship between the voltage and the acceleration that is being prepared to be monitored.

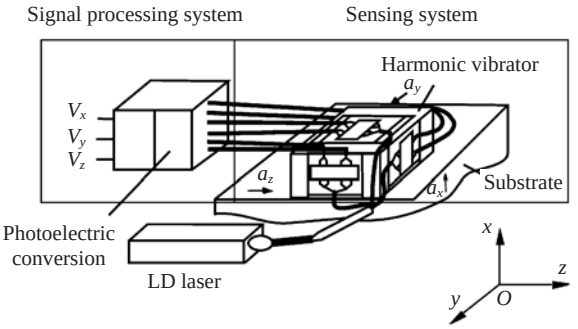

Fig.8 Schematic drawing of the three-component photoelastic waveguide accelerometer

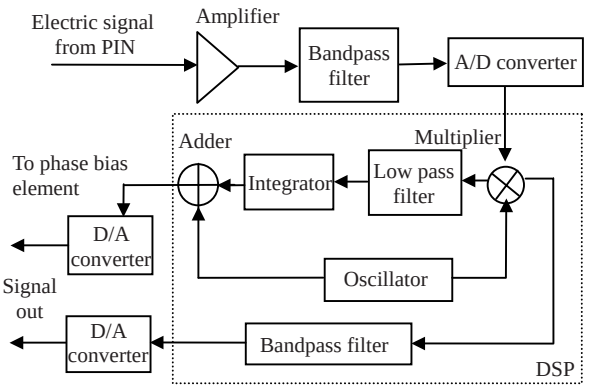

Fig.9 Signal processing system of the accelerometer

The frequency response characteristics of the accelerometer were measured using a vibration detection system (Fig.10). The output of the accelerometer as a function of the vibration frequency is shown in Fig.11, where Fig.11a and Fig.11b indicate the on- and cross-axis acceleration, respectively.

In Fig.11, two measured frequency spectra are shown for a=0.2g. The frequency spectrum curve for a=0.2g is flat in the range of about 100~3000 Hz as the useful frequency band, where the output voltage of the on-axis is a constant 147 mV. The output voltage of the cross-axis is lower at 21.3 mV.

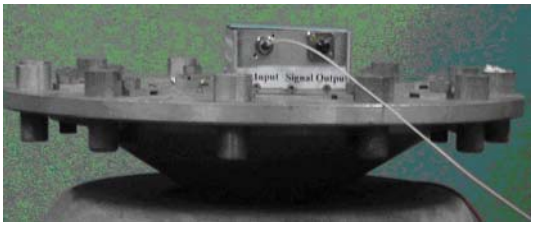

Fig.10 Photograph of the accelerometer on the shaker table

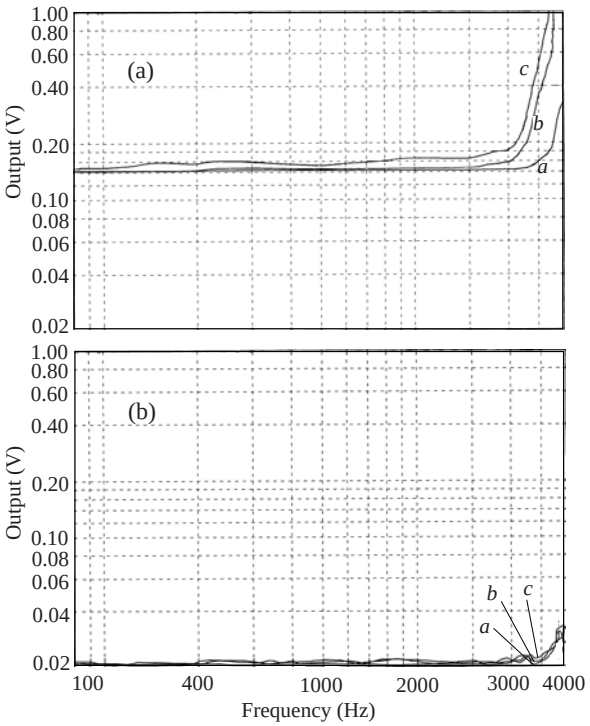

Fig.11 (a) On-axis frequency response curve; (b) Cross-axis frequency response curve

a, b, and c are the frequency response curves of the three M-Z interferences

CONCLUSION

In summary, the design and performance of a novel three-component hybrid-integrated optical accelerometer is described. The accelerometer is made up of three unidirectional sensing elements. Each element is based on the Mach-Zehnder interferometer, the design of which can restrict the vibration along only one direction to enhance the on-axis response and weaken the cross-axis response. By multiplexing three orthogonal unidirectional elements the accelerometer can obtain the three components of the vibration signal simultaneously. The accelerometer shows good linear frequency responding characteristics when the frequency is below 3000 Hz. The accelerometer also shows good stability and consistency. Experimental results indicate that the outputs of the on- and cross-axis are 147 and 21.3 mV, respectively. Such an accelerometer is suitable for vibration sensing in high-accuracy seismic exploration.

References

Burcham, K.E., de Brabander, G.N., Boyd, J.T., 1992. Micromachined Silicon Cantilever Beam Accelerometer Incorporating an Integrated Optical Waveguide. Proc. SPIE, **1793**:12-18. [doi:10.1117/12.141218]

Cole, J.H., Danver, B.A., Bucaro, J.A., 1982. Synthetic-heterodyne interferometric demodulation. *IEEE J. Quant. Electron.*, **18**(4):694-697. [doi:10.1109/JQE.1982.1071560]

Dandridge, A., Tveten, A.B., Giallorenzi, T.G., 1982. Homodyne demodulation scheme for fiber optic sensor using phase generated carrier. *IEEE J. Quant. Electron.*, **18**(10):1647-1653. [doi:10.1109/JQE.1982.1071416]

Dubey, V.N., Crowder, R.M., 2006. A dynamic tactile sensor on photoelastic effect. *Sensors and Actuators A*, **128**(2):217-224. [doi:10.1016/j.sna.2006.01.040]

Guo, D.G., Wang, W.J., Lin, R.M., 2004. Extrinsic Fabry-Perot Pressure Sensor Using Single Deeply Corrugated Diaphragm Technique. Proc. SPIE, **5346**:15-26. [doi:10.1117/12.516589]

Kiesel, S., van Vickle, P., Peters, K.J., Hassan, T., Kowalsky, M., 2006. Intrinsic Polymer Optical Fiber Sensors for High-strain Applications. Proc. SPIE, **6167**, Article 13, p.1-11.

Llobera, A., Plaza, J.A., Salinas, I., Berganzo, J., Garcia, J., Esteve, J., Domínguez, C., 2004. Technological aspects on the fabrication of silicon-based optical accelerometer with ARROW structures. *Sensors and Actuators A*, **110**(1-3):395-400. [doi:10.1016/j.sna.2003.10.053]

Ma, T.W., Zhao, W.B., Liu, J.M., 2007. A MEMS Vibration Sensor Based on Mach Zehnder Interferometers. Proc. SPIE, **6529**:2C-1. [doi:10.1117/12.715780]

Pavelescu, L., 2001. Simplified Design Relationships for Silicon Integrated Optical Pressure Sensors Based on Mach-Zehnder Interferometry with Antiresonant Reflecting Optical Waveguides. Proc. Semiconductor Conf., **1**:201-204. [doi:10.1109/SMICND.2001.967446]

Su, W., Gilbert, J.A., Morrissey, M.D., Song, Y.H., 1997. General-purpose photoelastic fiber optic accelerometer. *Opt. Eng.*, **36**(1):22-28. [doi:10.1117/1.601165]

Tang, D.L., Chen C.H., Cui, Y.M., Ding, G.L., Wang, J.H., Xie, J.Z., 2005. Spring system of three-component photoelastic fiber optic accelerometer. *J. Tianjin Univ. Sci. Technol.*, **38**(1):61-64 (in Chinese).